Advanced Steel Construction – Vol. 21 No. 6 (2025) 520–529
DOI:10.18057/IJASC.2025.21.6.5

PARAMETRIC STUDIES ON BENDING CAPACITY OF MECHANICAL JOINTS USING CONCRETE-FILLED STEEL TUBES

Vay Siu Lo [1, 2] and Canh Tuan Nguyen [1, 2, *]

[1] *Ho Chi Minh City University of Technology (HCMUT)*
[2] *Vietnam National University Ho Chi Minh City (VNU-HCM), Ho Chi Minh City, Vietnam*
* *(Corresponding author: E-mail: ctnguyen@hcmut.edu.vn)*

ABSTRACT

This study aimed to conduct an in-depth analysis of mechanical joints using a Concrete-Filled Steel Tube (CFST) for steel tube structures under bending. A series of parametric analyses were performed using finite element models. A conventional theory of CFST structures was applied to calculate the bending resistance of the joint. A key finding of this research was the equivalent strut-tie model to determine the local acting forces in the joint. The internal stress distribution within the concrete core was investigated to define effective areas for the components in compression and tension. Based on analysis results, this study proposed design proportions for the length-to-diameter ratio and the thickness ratio between the connecting steel tube and the main steel tubes. The influence of concrete strength, reinforcement ratios, and the use of shear connectors to prevent slip on the load-bearing capacity were also successfully examined. These findings are critical for simplifying construction practices and optimizing joint performance that might enable more effective and efficient use of CFST in various structural applications. This research revealed the potential of such innovative joint designs to significantly improve the construction method that requires rapid, reliable, and cost-effective solutions.

ARTICLE HISTORY

Received: 14 February 2025
Revised: 13 June 2025
Accepted: 15 June 2025

KEYWORDS

Bending capacity;
Circular steel tube;
Concrete-filled steel tube;
Mechanical joint;
Steel bridge

1. Introduction

Steel tubes are fundamental in structural engineering for their strength, durability, and flexibility [1], with demonstrated high ductility under seismic loading in bridges [2, 3]. Innovations include multiple-pipe bridge columns on varying foundations [4] and extensive use in offshore wind foundations, where steel pipe piles have been experimentally validated [5], supported by theoretical design and static tests for axial and uplift capacity [6], as well as connection analyses for single-pile turbines [7, 8].

Concrete-filled steel tubular (CFST) structures combine material and construction efficiency with fire resistance and environmental benefits [9]. Recent FEA studies have characterized their flexural behavior and stress-strain distributions, leading to strut-tie models for pure bending [10, 11], while experimental comparisons have refined design specifications for bending performance [12, 13]. Advancements in construction technology focus on rapid construction, prefabrication, modular structures, and innovative connection methods for steel pipe columns [14-16]. Advances in prefabrication and modular construction have spurred innovative connections, from bolted CFST girders [17] to mechanical joints like "High-Mecha-Neji" threaded sleeves [18], KASHEEN bolt assemblies [19], and tooth-and-pin mechanisms [20], and slip-joint solutions for offshore monopiles [7, 8]. Despite these developments, on-site welding and complex fabrication still hinder quality consistency and cost reduction in CFST jointing.

Studies on CFST structures involving lightweight aggregate concrete (LAC) and square steel tubes have also provided important foundations for the development of innovative CFST applications. Zhongqiu et al. [21] examined the flexural behavior of LAC-filled steel tubes (LACFST), demonstrating that LAC can maintain effective composite action with the steel tube while reducing structural self-weight. Their results confirmed that LACFST members possess reliable moment capacity and stiffness, and they proposed analytical methods verified through finite element analysis. In a separate study, Li et al. [22] explored the seismic performance of high-strength concrete-filled high-strength square steel tubes (HCFHSTs) under cyclic pure bending. Their experiments and numerical simulations revealed excellent ductility, energy dissipation, and flexural stiffness, even under high-strength material configurations. Further, Yang et al. [23] introduced reinforced hollow square CFSTs (RHCFSTs), integrating prestressed concrete cores and additional reinforcement. Their findings highlighted improved flexural capacity, delayed crack propagation, and enhanced ductility. These studies collectively demonstrate that varying the core concrete material and steel tube geometry significantly influences CFST behavior. Their insights serve as a valuable reference for developing new CFST-based mechanical joints, especially where construction efficiency, weight reduction, and flexural performance are critical.

Recent studies in structural engineering have refined the strut-and-tie model (STM) for designing deep beams in reinforced concrete structures, ensuring safety, and optimizing material use. Various research has enhanced the STM, proposing modifications to codes and innovative methods for design accuracy and reliability. Park et al. [24] introduced an advanced STM method incorporating constitutive laws for cracked reinforced concrete to provide superior capacity estimates for deep beams compared to existing codes. Other studies have recalibrated STM effectiveness factors based on concrete strength and shear span-to-depth ratios, aligning with experimental data and codes like ACI Code-08 and the UK CIRIA Guide #2 [25]. Research on shear design provisions for D-regions in beams highlighted the transition from conventional sectional methods (CSM) to STM, suggesting integration for certain beam configurations [26]. Tuchscherer et al. [27] evaluated deep-beam tests, proposing modifications to ACI 318 and AASHTO LRFD provisions to balance conservatism and accuracy.

The current research was built on previous studies, proposing a new mechanical joint using CFST that maintained bending capacity comparable to steel pipe columns without the joint [28]. This joint can be used for CFST girders, steel pipe piles, and steel pipe columns, aiding accelerated construction. Parametric studies were conducted using finite element models to analyze mechanical joints in CFST structures under bending. The conventional CFST theory was applied to calculate bending resistance, while a new finding assessed local resistance using the strut-tie model of a deep beam. Internal stress fields within the concrete core were investigated to propose effective areas for defining component resistances under compression and tension.

The study proposed design proportions for the length-to-diameter and thickness ratios between the connecting tube and main steel tubes. It examined the influence of concrete strength, reinforcement ratio, and shear connectors on load-bearing capacity. Overall, this research presents a simple, cost-effective mechanical joint using CFST, eliminating the need for site welding or expensive joint solutions while ensuring construction progress.

This paper was organized as follows: Section 2 provided an overview of the proposed mechanical joint utilizing concrete-filled steel tubes, introducing the strut-and-tie model as a framework for analysis. Section 3 delved into the details of the finite element model employed for CFST simulations, along with validation procedures to ensure accuracy. Section 4 presented a comprehensive parametric study, investigating the effects of various factors on joint performance, including effective length, connecting tube thickness, concrete compressive strength, and reinforcement ratio. In Section 5, design proportions and recommendations were derived from the analysis results. Finally, the concluding Section 6 summarized the key findings and offered insights into future research directions.

2. Mechanical joint using concrete-filled steel tube

2.1. The proposed CFST joint

This study proposes a straightforward and cost-effective mechanical joint using CFST that could eliminate the need for site welding or expensive joint solutions while still ensuring construction progress. The continuity of the structure was maintained by using a connecting steel tube to link the two main steel tubes. The rigidity of the connecting tube was enhanced by filling it with reinforced concrete. Additionally, shear connectors might be applied to improve the interaction between the main steel tubes and the joint, ensuring continuity during the load-bearing process. Axial force, shear force, and bending moment can be transferred between the two main tubes through the mechanical joint. The length of the connecting tube was a key parameter affecting the joint's performance. Therefore, this paper aimed to investigate the effects of various parameters on the bending capacity of mechanical joints such as connection length, tube thickness, compressive strength of the concrete core, steel reinforcement ratio, and dowel interactions of shear connectors. Through parametric studies, considerations and proportions were proposed to simplify design practices.

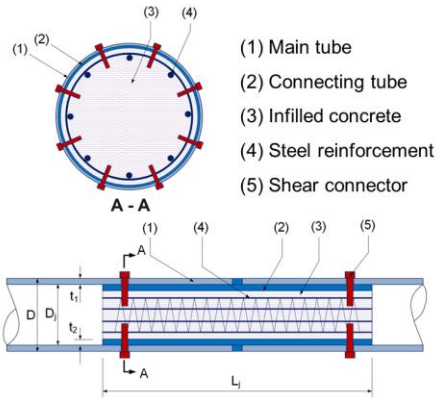

Fig. 1 Steel tubes with a mechanical joint using a concrete-filled steel tube [28]

Figure 1 illustrates the composition of the proposed mechanical joint using a reinforced concrete-filled steel tube where D is the outer diameter of the main tube, D_j is the outer diameter of the connecting tube, t_1 and t_2 are the thicknesses of the main tube and the connecting tube respectively. The connecting tube could be prefabricated and filled with concrete at the factory, then transported to the construction site for erection. This joint could provide load-bearing capacity immediately after installation. For piles constructed using the rotary drilling method or pullout piles, shear connectors could be applied to ensure that torque or uplift force are transmitted effectively through the joint.

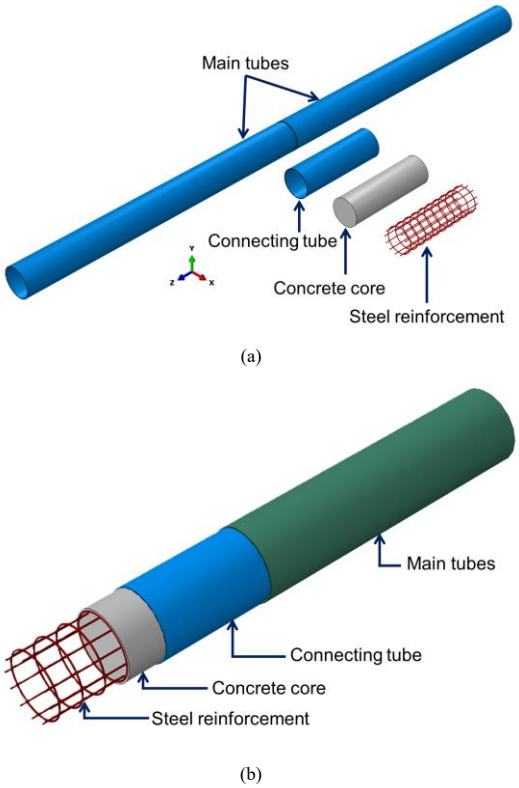

Fig. 2 Illustration of the mechanical joint model

The simple principal mechanism of the joint is to transmit internal forces between two main steel tubes, effectively functioning as a continuous steel tube. Such performance is achieved through frictional interaction between the inner surface of the main tubes and the outer surface of the connecting tube. Ideally, the outer diameter of the connecting tube would fit the inner diameter of the main tubes. To simplify construction and installation, however, the outer diameter of the connecting tube could be 1 mm to 2 mm smaller than the inner diameter of the main tubes. By analogy with a fitting connection, the main tubes could be heated before installing the connecting tube to improve fitting contact. Fig. 2 illustrates a three-dimensional model of the mechanical joint structure, including a breakdown of its components and a cross-sectional view that details the internal arrangement of the joint. The concrete core could improve local stability for the connecting tube under compressive stress, while the reinforcing steel might enhance the tensile capacity and prevent cracks in the concrete core under tensile stress.

2.2. Bending strength of mechanical joint

Theories of conventional CFSTs under bending can be employed to verify the performance of a mechanical joint with a CFST. The plastic-stress distribution method could be applied to determine the bending capacity of the mechanical joint. This method has been recommended as an adequate solution due to its simplicity and accuracy for CFST structures [15, 29].

The theory for calculating the flexural resistance of CFST has been successfully developed and included in recent design specifications [30-33]. Fig. 3 illustrates the Plastic Stress Distribution Method (PSDM) of a CFST cross-section with steel reinforcement at a critical state. Stress distributions in the steel tube, concrete core, and steel reinforcement are also defined to satisfy the equilibrium conditions under external bending moments transmitted from the main tubes.

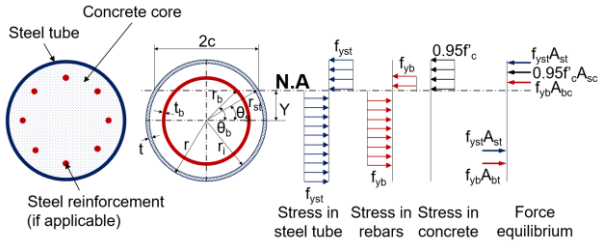

Fig. 3 Plastic stress distribution model of a CFST cross section [30]

The total bending resistance is combined from the contributions of the steel tube, concrete core, and reinforcing bars. By applying the plastic stress distribution method and ignoring axial force, the bending capacity is determined through the equilibrium condition between the external bending moment and the internal bending moments generated by the plastic forces at the centroid of the sectional components. The nominal bending resistance can be calculated as follows [30]:

$$M_n = 0.95 f_c' \left[\left(r_1^2 - y^2 \right) - \frac{c^2}{3} \right] + 4 f_{yst} t c \frac{r_{st}}{r_1} + 4 f_{yb} t_b c_b r_b \tag{1}$$

where,

$$\begin{aligned} &r_{st} = r - t/2; \quad \theta_b = \sin^{-1}\left(y / r_b\right); \quad c_b = r_b \cos\theta_b; \\ &\theta_s = \sin^{-1}\left(y / r_{st}\right); \quad c = r_i \cos\theta_s; \quad t_b = n A_b / 2\pi r_b \end{aligned} \tag{2}$$

in which A_b is the area of a typical steel bar comprising the internal reinforcement (mm^2); c is one-half the chord length of the tube in compression (mm); c_b is one-half the chord length of a notional steel ring equivalent to the internal reinforcement in compression (mm); f_{yb} is yield stress of steel bar (MPa); f_{yst} is yield stress of steel tube (MPa); f_c' is compressive strength of concrete core (MPa); n is number of internal steel reinforcing bars; r is radius to the outside of the steel tube (mm); r_b is radius to the center of the internal reinforcing bars; r_i is radius to the inside of the steel tube (mm); r_{st} is radius to the center of the steel tube (mm); t is the wall thickness of the tube (mm); t_b is the wall thickness of a notional steel ring equivalent to the internal reinforcement (mm); y is distance from the center of the steel tube to the neutral axis (mm); θ_b is angle used to define c_b (rad), θ_b shall be taken as $\pi/2$ if y/r_b is greater than 1 and θ_b shall be taken as $-\pi/2$ if y/r_b is less than -1 (rad); θ_s is angle used to define

c (rad).

This study discovered that the mechanical joint could behave like a deep beam if the ratio between the length of the joint and the diameter of the tube is less than 3.0 [25]. To evaluate the local load-bearing capacity of a deep beam structure, a theory of strut-and-tie model was applied.

2.3. Strut-and-tie model for local resistance estimation

The strut-and-tie model (STM) is a design method used in structural engineering to simplify the complex stress distribution in concrete structures into truss-like models. This model is particularly useful in areas of structures that are complex to analyze using traditional methods, such as beam-column joints, deep beams, corbels, dapped beams, and pile caps. Struts are compression elements carrying compressive stresses across a direct line between nodes. Ties are in tension connecting nodes where tensile forces are expected, effectively holding the structure together under tensile stress. Nodes are the junction points where struts and ties meet. Nodes transfer forces between struts and ties and are critical for the stability of the STM. This method aligns more with actual stress flow in irregularly shaped and heavily loaded parts of structures, offering a more rational approach than traditional beam theory.

The conventional STM is used to simplify complex stress fields in concrete structures by replacing them with truss-like systems of compression struts, tension ties, and nodes. Traditionally, this approach has been applied to reinforced concrete structures, capturing the flow of forces through concrete members. However, in this study, an equivalent STM is proposed to model the local load-bearing capacity of steel mechanical joints in CFST structures. Unlike conventional STM, this model accounts for nonlinear radial pressure distributions and friction forces that develop at the interface of steel tubes in the joint, which are not typically considered in concrete STM applications.

The equivalent STM captures the direct load transmission between steel tubes and the concrete core, reflecting how bending moments in the main tubes create concentrated radial pressures that form struts and ties within the joint. This adaptation allows us to better understand the local mechanical behavior of interference-fit steel joints under combined bending and compression, filling a gap not addressed by traditional STM. This model's novelty lies in its ability to incorporate these localized effects and frictional behavior in steel joints, providing a more realistic assessment of load-bearing capacity in CFST connection.

This study proposed an STM with two concentrated loads to investigate the local load-bearing capacity of the mechanical joint based on the deep-beam theory similar to previous research [24, 25]. The fit connection between outer tubes and an inner tube with different diameters can be considered as a shrink-fit joint without initial contact pressures on the fitting. Due to the small gap between the main tubes and the connecting tube, the joint is fixed and exhibits linear behavior. The interference connection may lead to nonlinear behavior with large angular deformation of the main tubes; pressure concentrations then develop at the joint edges. The friction forces induced by radial pressure could prevent relative slip between the fitting surfaces which may lead to failure of the joint [34]. Fig. 4a presents a proposed load distribution model within the mechanical joint. Bending moments M in the main tubes are transformed into equivalent radical pressure regions which generate concentrated couples N. In this study, the pressures in the longitudinal direction were assumed to be linearly distributed in the range of $L_j/6$ as an active length from edges of the main tubes and connecting tubes. Similar pressure distribution models with active lengths were introduced to investigate the effects of the overlap length on the bending capacity of the slip joint [35, 36].

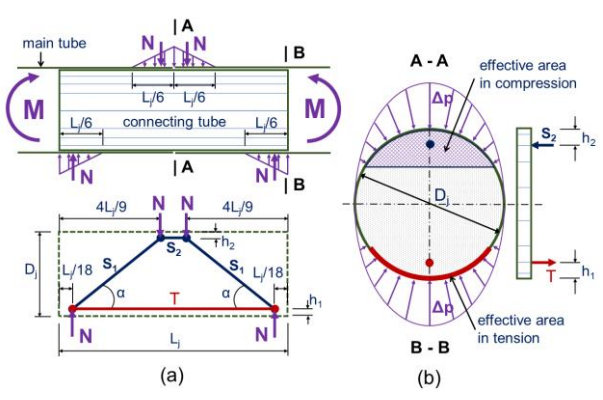

Fig. 4 Proposed strut-and-tie model and equivalent radial pressure in tube section

In the vertical section, the radial pressure is nonlinearly distributed along the half circumference of the connecting tube (see Fig. 4b). To investigate the effects of friction forces, the magnitude Δp can be determined based on similar theory developed from a previous study [34]. From the model, struts S_1 and S_2 in compression and a tie T in tension are identified. It is assumed that internal loads are transferred directly between nodes through the struts in the concrete core.

The tie force T is assumed to be mostly generated along the bottom fiber of the connecting steel tube, neglecting the contributions of the concrete core and reinforcing bars. Strut force S_2 is generated in the top fiber of the cross section. Distances from centers of the tie force T and strut force S_2 to corresponding extreme fibers are h_1 and h_2, respectively. From the force equilibrium conditions, the component struts and tie can be defined as:

$$S_1 = N / \sin\alpha \tag{3a}$$

$$S_2 = T = N / \tan\alpha \tag{3b}$$

where, $\alpha = \text{atan}\left[\left(D_j - h_1 - h_2\right)/\left(7L_j/18\right)\right]$; N is the acting forces on the joint obtained from the bending moment equilibrium condition, $N = 18M/(7L_j)$.

To completely transmit bending moment between main tubes, the local load-bearing capacity of the mechanical joint should be examined by comparing the internal forces obtained from Eqs. (3a) and (3b) with the component strengths formed by effective areas. In this study, stress distributions in the concrete core and the connecting tube were observed to investigate effective areas in tension and in compression of the CFST cross section.

3. Finite element modeling

To examine the behavior of mechanical joints under pure bending, a simply supported beam model was employed with two concentrated loads P positioned at a distance a from the supports. This loading configuration eliminated shear forces and created a region of a constant bending moment between the two load points. The span length was set to 20 times the diameter of the main tubes. Fig. 5 illustrates the loading arrangement, as well as the corresponding bending moment and shear force diagrams. In this scenario, the connecting tube was subjected only to a pure bending moment, $M = Pa$. This setup provided perfect conditions to study the performance of mechanical joints, focusing on the transition of internal moments to ensure the bending capacity of the entire structure.

This type of loading scheme has also been adopted in previous studies to evaluate the flexural behavior of CFST members. Notably, Guochang Li et al. [22] and Zhi-Jian Yang et al. [23] employed similar four-point bending arrangements to generate a pure bending region, enabling accurate assessment of moment resistance and structural ductility in high-strength square CFST beams. The consistency in test setup across studies further validates its effectiveness in capturing the essential flexural characteristics of CFST-based structural systems.

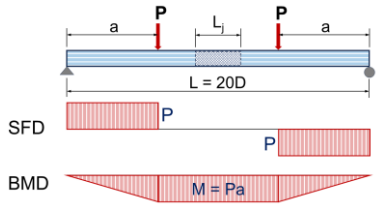

Fig. 5 Simply supported beam under two-point loading condition

A series of finite element models of steel tubes with a mechanical joint using a concrete-filled steel tube were simulated using the ABAQUS analysis software [37]. Fig. 6 illustrates a finite element model of a steel tube beam with a mechanical joint using a concrete-filled steel tube. The joint was located between two concentrated loads spaced two meters apart. To prevent local buckling, bearing stiffeners were created at both supports and at locations of the concentrated loads. A one-millimeter gap was created at the edges of the main steel tubes to model interactions between two tubes. Inside the joint, a smaller-diameter steel tube was embedded and filled with a reinforced concrete core.

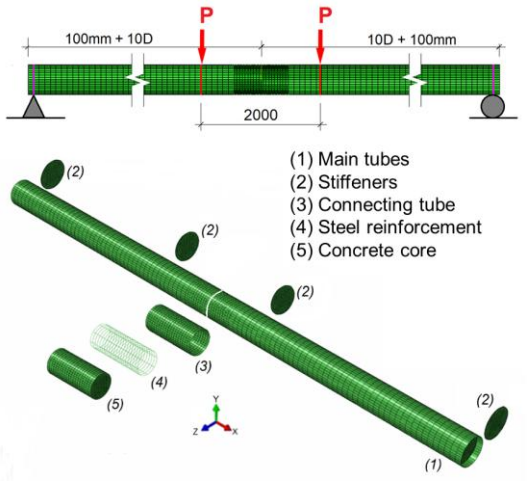

Fig. 6 Finite element model of a steel tube beam with mechanical joint using CFST [28]

3.1. Element types

The main steel tubes, connecting steel tube, and bearing stiffeners were modeled using 4-node shell elements (S4R), while the general-purpose linear brick element (C3D8R) with 8 nodes was employed to simulate the concrete core. Reinforcement bars within the concrete core were modeled as truss elements (T3D2), which could be embedded into the concrete core. The interactions between the two main tubes (see Fig. 7a), between the main tubes and the connecting tube (see Fig. 7b), and between the connecting tube and the concrete core (see Fig. 7c) were modeled using GAP elements, simulating bearing interactions and friction sliding. GAP elements work by incorporating contact mechanics into the finite element model. When the gap between two surfaces closes, the elements apply contact forces that can include both normal and tangential components. The normal component of the contact force typically simulates the bearing pressure, while the tangential component models the frictional resistance to sliding. This dual capability allows GAP elements to accurately reproduce the complex interactions such as those found in mechanical joints, bearings, and other structures where surface contact and friction are critical.

To mitigate slippage and evaluate the impact of the connection between the concrete core and the steel tube, shear connectors were modeled using rigid links in the form of tie interactions. These connectors were arranged along the circumference of the steel tube near the rear end of the connecting steel tube. By employing tie interactions, the shear connectors effectively constrain relative movement between the steel tube and the concrete core, thereby enhancing the structural integrity and load transfer efficiency of the composite system.

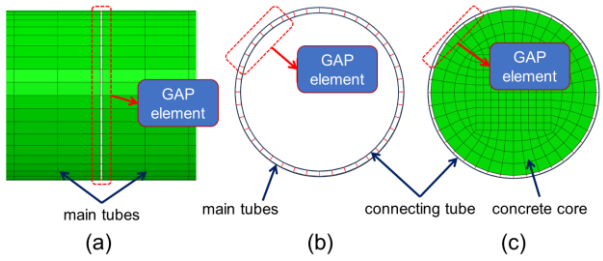

Fig. 7 Modeling surface interactions using GAP elements [28]: (a) edge interaction; (b) tube-tube interaction; (c) tube-core interaction.

Several studies have successfully applied and validated the use of GAP elements in simulating the behavior of concrete-filled steel tube structures. A friction coefficient 0.47 for the GAP element between the steel tube and the concrete core has been proposed based on research by Baltay et al. [38, 39]. Jiho et al. also conducted a series of parametric analyses and successfully validated the simulation method using GAP elements for the interaction between steel and concrete surfaces [12, 15]. For static friction of steel-on-steel contact, the friction coefficient could be estimated between 0.6 and 0.8 in dry air and without lubrication [40-43]. In practical construction, steel tubes are usually coated with a thin prime layer using epoxy-based painting for corrosion protection. The coating layer significantly reduces friction coefficients between two coated steel surfaces. Cabboi et al. [8] confirmed that the presence of the two-coat layer might be the reason for a drastic friction reduction from 0.6 - 0.8 to a possible 0.1 - 0.35 range in slip joint. In this study, a friction coefficient of 0.45 has been proposed for steel-on-steel contact surface with slightly coated layers. This value is also consistent with the friction coefficient proposed in Article 6.13.2.8 by the AASHTO standards when calculating the slip resistance of the bolted connection [30].

The number of meshed elements is crucial to ensure reliable finite element analysis results. In a similar study, Moon et al. [12] also demonstrated that using a minimum of twenty elements along the circumference of a steel tube would yield accurate results. In this study, the steel tubes were divided into forty elements along the circumference to secure the accuracy of analysis results (see Fig. 7). In the longitudinal direction, the region of the joint was meshed more finely than other regions, as illustrated in Fig. 6. The width of the elements within the joint will be half as large as those in other regions. This meshing approach aligned with findings from previous research.

3.2. Material properties

Nonlinear material analysis as well as large deformation analysis were applied to accurately investigate and evaluate the behavior of the structure. To simulate the behavior of the steel tube and reinforcing steel materials, this study employed a three-linear material model that represented the stages of elasticity, full plasticity, and strain hardening. Fig. 8 illustrates the general stress-strain curve for the steel material, assuming an elastic modulus E_s = 200,000 MPa and a Poisson's ratio υ_s = 0.3. The yield strength f_y was defined corresponding to the yield strain ε_y, with the plastic state maintained until the strain reaches 10 ε_y. The ultimate strength f_u was identified at a strain ε_u = 0.1. This steel material model has also been applied and successfully validated in previous studies [12, 13]. In this study, the steel tube had a yield strength f_y = 345 MPa and an ultimate strength f_u = 490 MPa, while the reinforcing steel had a yield strength f_y = 400 MPa and an ultimate strength f_u = 570 MPa.

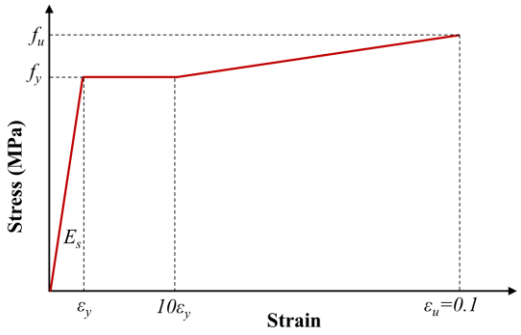

Fig. 8 Material models for steel tubes and steel reinforcement

Recent advancements in concrete modeling have successfully developed damage mechanics and plasticity theory to enhance the predictive accuracy of concrete behavior under various loading conditions. Several studies have proposed different constitutive models emphasizing the non-linear analysis of concrete through improved yield criteria and damage variables that capture both tensile and compressive states. New damage-plasticity approaches were presented to model concrete failure under general triaxial stress covering tension, shear, and multiaxial compression with distinct levels of confinement [44-47].

The nonlinear finite element analysis of concrete materials has been extensively studied in previous research. Moon et al. [12] applied concrete damage models to analyze concrete-filled steel pipe structures. Their research verified the accuracy of the uniaxial stress–strain relationship for unconfined concrete using a plastic failure model in conjunction with the GAP element. This approach effectively simulated the behavior of concrete-filled steel pipe structures through a series of nonlinear finite element parameter analyses. Achieving convergence can be challenging when fully incorporating the nonlinear behavior of concrete, making the choice of an appropriate material model crucial. In this study, the concrete damage plasticity model was adopted, following the work of Lubliner et al. [48] and Lee and Fenves [49]. This model effectively represents concrete behavior under various stress states, particularly when the confining stress remains below four to five times the concrete's compressive strength. Additionally, the dilation angle significantly affects the simulated response of concrete. Based on previous research and a parametric study conducted in this work, a dilation angle of 20 was selected.

The uniaxial stress–strain curve is presented in Fig. 9. In this study, the concrete grade C40 with f_c' = 27 MPa were employed to investigate effects of connecting length, thickness, and reinforcement ratio.

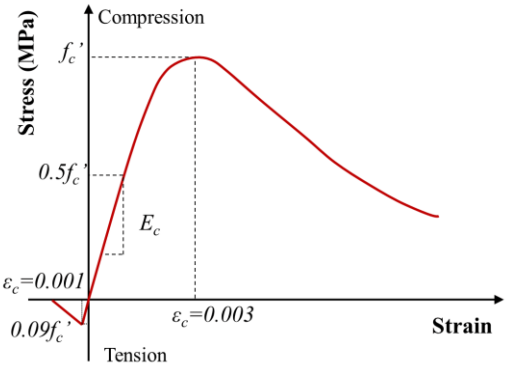

Fig. 9 Material models for infilled concrete

3.3. Bending strength of a steel tube

The mechanical joint was employed to successfully transmit bending moments between main tubes. This means that the joint must produce sufficient load-bearing capacity to prevent failure before main tubes reach the critical bending strength.

This study proposes a method to identify the critical bending moment of the main tubes based on the moment-rotation relationship diagram. The bending strength of the jointless steel tube was used as a benchmark for comparative studies. From finite element analysis results, the corresponding bending moment was determined by using the rotation angle value at the first yield, ϕ_y. The plastic bending moment of a hollow steel tube M_p is defined as:

$$M_p = \lambda M_y = \lambda Z f_y \tag{4}$$

where, M_y is the yielding bending moment, $M_y = Zf_y$; Z is the elastic section modulus of the steel tube; f_y is the yield stress (MPa); λ is shape factor of the section, λ = 1.27 for a circular tube [50].

For a simply supported beam subjected to two concentrated loads (illustrated in Fig. 7), the total rotation angle at a support at first yield is defined as follows:

$$\phi_y = M_y(L-a)/(2EI) \tag{5}$$

where a is the distance from concentrated loads to supports.

3.4. Comparison and verification of bending strength

Previous research has demonstrated the effectiveness of mechanical joints with concrete-filled steel tubes for steel pipe columns. The verification of the bending strength of steel pipe columns using mechanical joints was conducted through finite element analyses by comparing the results to theoretical calculations. The study employed a series of finite element models with varying diameters and joint configurations to simulate the bending behavior under applied loads [28].

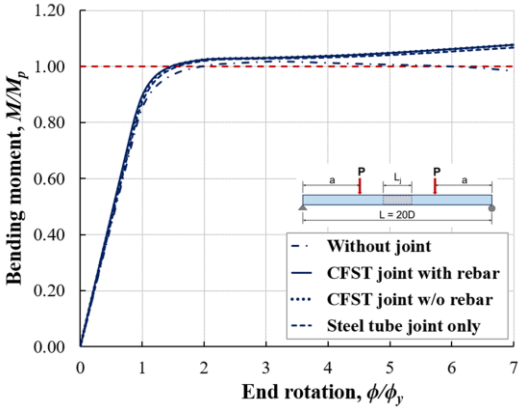

(a) D = 200 mm, L_j = 1000 mm

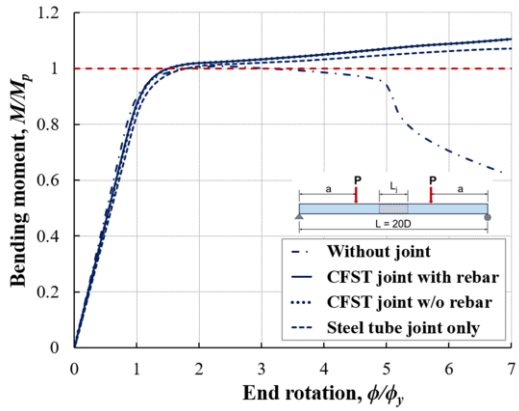

(b) D = 350 mm, L_j = 1000 mm

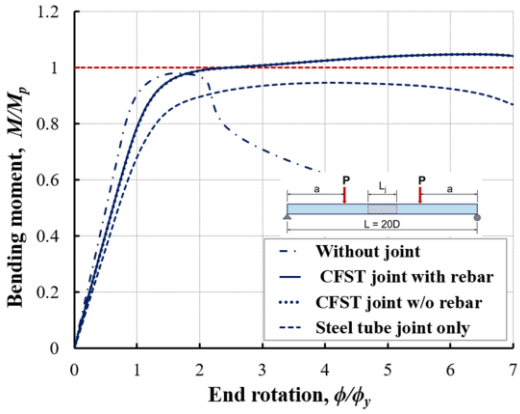

(c) D = 500 mm, L_j = 1000 mm

Fig. 10 Comparison of bending capacity between steel tubes with and without joint

Figure 10 presents the comparative results of the bending strength between steel pipes with and without mechanical joints using CFST. The plastic bending moment M_p from Eq. (4), and the rotation angle at first yield of the tube section, ϕ_y, from Eq. (5) were used as benchmarks for comparison. Furthermore, the comparison was also conducted between joints with and without rebar reinforcement to evaluate their contribution to the overall resistance of the connection. The mechanical joints, filled with reinforced concrete, demonstrated significant improvements in bending capacity compared to pipes without joints. Comparative analysis showed that the proposed mechanical joints could increase the bending strength of steel pipes by up to 21.6%. Stress distributions and deformation patterns were closely observed, indicating that the concrete core within the joint effectively prevented local buckling and contributed to the overall joint rigidity [28]. The findings from this preliminary study serve as the foundation for the current research, where the derived results will be systematically compared with Eqs. (4) and (5) to assess the validity of mechanical joints in steel pipe columns. A detailed discussion on failure mechanisms, including stress distribution within the concrete core and steel pipe connections, will be presented in the following section.

4. Parametric studies and verification

This study conducted a series of parametric analyses using finite element modeling to investigate and assess the efficiency and optimal performance of mechanical joints. The goal was to provide recommendations for the geometric design of these joints with considerations of key geometric parameters including tube diameter, length of the joint, tube thickness, concrete strength, reinforcement ratio, and anchoring effects.

4.1. Effective length of the mechanical joint

For double-tube mechanical joints, the diameter of the connecting tube is determined by the inner diameter of the main tubes. Consequently, this parameter was not examined in this study. Instead, the focus was on investigating the relationship between the main tube diameter and the joint length.

As discussed in the theoretical section, the length of the connecting tube affects the magnitude of the equivalent couple derived from the bending

moment in the main tubes. This couple is considered as an external force acting on the connecting tube. The longer the joint length is, the smaller the magnitude of the couple acts on it. The length of the connecting tube plays a crucial role in ensuring the joint's functionality in transmitting the bending moment from the main tubes through the connecting tube guaranteeing that the joint's load-bearing capacity is always greater than or equal to the bending capacity of the main steel tubes. The joint's load-bearing capacity depends on the frictional interaction on the contact surface between the main tubes and the connecting tube. Such frictional force limits slip and ensure the transmission of the bending moment between the main tubes and the connecting tube. The frictional force depends on the magnitude of the couple acting on the connecting tube and the effective contact surface area.

Table 1 presents the geometric characteristics of the finite element models used for parametric analyses to investigate the impact of connecting length on the load-bearing capacity of the entire structure. Main steel tubes were examined with three different diameters of 200 mm, 350 mm, and 500 mm. The effective span length of the main steel tubes was set to 20 times its diameter. In this study, the length of the connecting tube L_j varied from 200 mm to 1,000 mm at intervals of 100 mm. A total of 27 models were employed in finite element analyses corresponding to different diameters of the main steel tubes. The connecting tube was set to have equal thickness to the main tubes. The models were loaded until failure to construct perfect moment-rotation relationship curves. The bending resistance and deformation of the joints will be examined to assess the performance with different joint lengths. To compare bending resistances, the rotation angle ϕ_y from Eq. (5) will be used as a reference value to determine the corresponding bending moments from the moment-rotation relationship curves for each case.

Table 1
Properties of finite element models with varying length of joint

Model	Main tubes					Connecting tube	
	D (mm)	t (mm)	L (mm)	M_y (kN.m)	ϕ_y (rad)	t_j (mm)	L_j (mm)
D200	200	6	4,000	59.41	0.02591	6	varied
D350	350	8	7,000	247.88	0.02231	8	varied
D500	500	8	10,000	516.46	0.02077	8	varied

The results from the D350 model analysis were used to illustrate the method for determining bending resistance. Fig. 11 presents diagrams of bending moments and rotation angles for various lengths of the joint characterized by the ratio $k = L_j / D$. The horizontal axis represents the ratio between the rotation angle from finite element analyses and that from Eq. (5) for D350 model. The vertical axis illustrates the ratio between the equivalent bending moment computed from the concentrated force P and the distance a from the loaded points to supports and that from Eq. (4). The rotation angle ϕ_y was taken as the standard to determine the corresponding bending resistance for different lengths of the joint. Results indicated that the length of the joint significantly influences the performance and the bending stiffness of the entire structure. Decreasing in length of the joint increased slip between the main tube and the connecting tube causing larger deformation of the joint and reducing efficiency in transmitting bending moments. At rotation angle ϕ_y , as the ratio $k = L_j / D$ increases from 0.57 to 2.86, the ratio of bending resistance M / M_y also increases from 0.32 to 1.11. The bending resistance of steel tubes with a joint length ratio L_j / D = 2.86 is equivalent to that of the steel tube without a joint, with an error of 2.4%. The bending stiffness of the steel tube could be determined based on the slope of the moment-rotation relationship curve. It was also found that bending stiffness of the structure increased with increasing length of the joint.

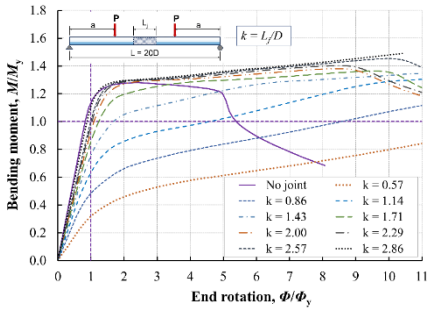

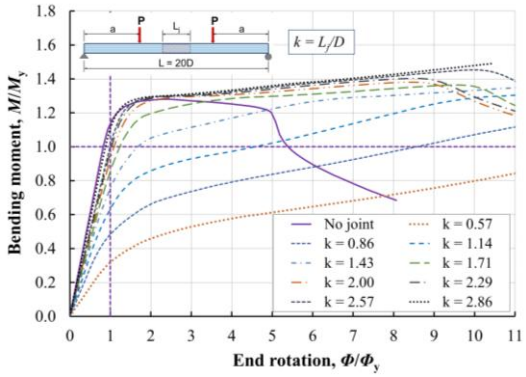

Fig. 11 Bending moment with various lengths of connecting tubes (D = 350 mm)

To investigate the effects of joint lengths on the bending resistance, Fig. 12 summarizes the analysis results of three models D200, D350, and D500. The *x*-axis represents the ratio of joint length to main tube diameter, while the *y*-axis shows the ratio of bending resistance from finite element analysis to the yield moment from Eq. (4). The analysis clearly revealed a correlation between bending resistance and joint length. All models performed linear variation in bending resistance when $L_j / D \leq 2.0$. Within the range $2.0 \leq L_j / D \leq 3.0$, larger diameters could provide faster increase in bending resistance to approach M_y . At L_j / D = 2.0, the differences in bending capacity of the analysis models and M_y were -9.2%, -7.4%, and +0.3% for models D200, D350 and D500, respectively. Models D350 and D500 could provide sufficient bending resistance when $L_j / D \geq 2.5$, while model D200 could only achieve M_y at L_j / D = 3.0. Based on these findings, it can be concluded that the optimal joint length L_j ranges between 2.5 and 3.0 times relative to the main tube diameter D. Therefore, this study recommends an ideal joint length L_j = 3.0 D for main pipe diameters ≤ 200 mm and L_j = 2.5 D for diameters > 200 mm in the design of the mechanical joints using concrete-filled steel tubes. In similar studies on a slip joint connection for single-pole transmission towers and offshore wind turbines using monopiles, the ideal overlap length has been successfully developed and suggested in design standards [50-53]. The overlap length of the slip joint is taken as 1.5 times the diameter which is consistent with findings from this study when the overlap length of a half joint is considered.

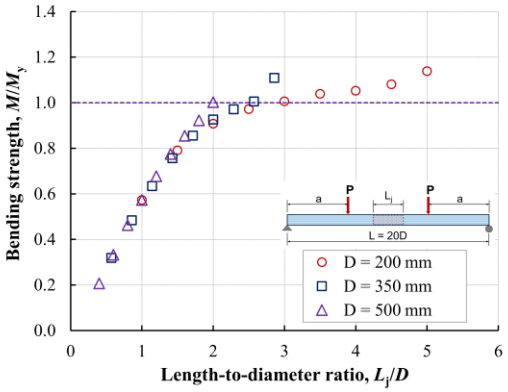

Fig. 12 Variation in bending strength with varying connecting length

In addition to examining the impact of joint length on bending resistance, this study also evaluated its effect on structural deformation, primarily influenced by the gap width between the two main tubes at the discontinuous section. Fig. 13 illustrates the gap width development at the joint section between the main tubes for various joint lengths from models D200, D350, and D500. The horizontal axis represents the ratio of joint length to diameter of the main tube, while the vertical axis represents the gap width relative to the diameter of the main tube at the bottom extreme fiber of the main tube. Results indicated that increasing joint length correlated with reducing gap deformation.

Results revealed that all models D200, D350, and D500 had a similar trend in gap width variation with different joint lengths. Gap width tends to approach 0.5% when $L_j / D \geq 2.5$. Therefore, global structural deformation under bending conditions can be secured by controlling expansion of the gap. The limiting joint length of L_j = 2.5 D suggested in this study is effectively to control gap development of the joint. Moreover, alternative solutions such as

employing shear connectors to enhance the interaction between main tubes, connecting tubes, and the concrete core can also mitigate gap expansion and global deflection. Effects of shear connectors will be explored in a separate follow-up study.

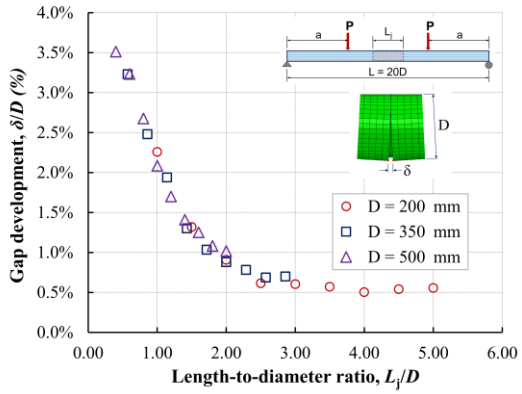

Fig. 13 Variation in gap width with varying joint length

4.2. Effective thickness of the connecting tube

The thickness of the connecting tube is also a critical parameter in the design of mechanical joints using concrete-filled steel tubes. This section investigates the effects of tube thickness on the bending resistance of the steel tube with the mechanical joint. The analysis aimed to propose simplified geometric parameters for the connecting tube thickness. Table 2 outlines the parameters of the finite element analysis models. The length of the joint is selected based on the effective length proposed earlier to maximize the structure's bending resistance. For models D200, D350, and D500, with connecting tube lengths of 600 mm, 900 mm, and 1000 mm respectively, the study explored the bending capacity as the connecting tube thickness varies from 2 mm to 14 mm at interval of 2 mm. This comprehensive investigation aimed to understand how changes in connecting tube thickness impact bending resistance.

Table 2
Properties of finite element models with varying thickness of connecting tube

Model	Main tubes			Connecting tube	
	D (mm)	t (mm)	L (mm)	L_j (mm)	t_j (mm)
D200	200	6	4,000	600	2 to 12
D350	350	8	7,000	900	4 to 14
D500	500	8	10,000	1,000	4 to 14

The thickness of the connecting tube directly impacts its local load-bearing capacity. Despite being filled with concrete, analyses revealed that the connecting steel tube contributed the most load-bearing capacity under both tensile stress and compressive stress. Fig. 14 illustrates how bending resistance of steel tubes varies with changes in pipe thickness. The horizontal axis denotes the ratio of connecting pipe thickness to main pipe thickness, while the vertical axis represents the ratio of bending resistance determined by finite element analysis to the yield moment from Eq. (4).

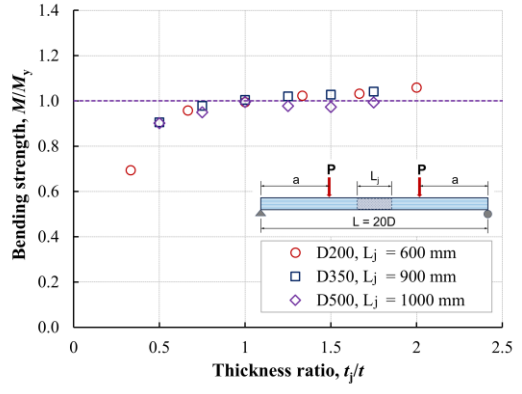

Fig. 14 Effect of thickness of connecting tube on bending strength

Results indicated a significant increase in bending resistance as the thickness increased. All models D200, D350, and D500 exhibited a consistent trend towards approaching the My value when the thickness of the connecting tube equaled that of the main tube ($t_j / t = 1.0$). Beyond this point, further increases in tube thickness did not yield substantial increases in bending resistance. Based on these findings, this study suggested that for optimal development of bending resistance, the ideal thickness for the connecting tube should equal that of the main steel pipe ($t_j = t$).

4.3. Effects of compressive strength of the concrete and reinforcement ratio

Previous studies revealed that infilled concrete provided a significant contribution to load-bearing capacity of the mechanical joint by improving local stability of the connecting tube [28]. However, the effects of compressive strength of the concrete on the bending capacity were not investigated. It was found that the concrete core could generate local compression strength under strut forces from the STM theory. Therefore, this study examined how compressive strength of the concrete core affected the performance of the joint.

Table 3
List of concrete material employed in parametric studies

Grade	C25	C30	C35	C40	C45	C50	C60	C70	C80
f_c' (MPa)	17	21	24	28	31	34	41	48	55

Table 3 presents data on various concrete types used to examine the impact of compressive strength on the bending resistance of joints. Finite element models employed a general material model, as shown in Fig. 9, to simulate concrete behavior. Compressive strength from grade C25 to C80 was considered in this study where grade C40 was selected as the benchmark for comparing bending resistance across different grades of concrete.

Analysis results indicated that the influence of concrete compressive strength on the bending resistance of the main tube was insignificant. Even at the lowest strength level, grade C25, joints almost provided sufficient bending resistance. Fig. 15 illustrates the analysis results, showing the relationship between compressive strength parameters where grade C40 represented the benchmark value, and the ratio of bending resistance derived from finite element analysis to the M_y value calculated using Eq. (4).

Most cases of failure were observed in the main steel tube due to local instability in the compression zone near the joint area. This study focused solely on main steel tubes connected by mechanical joints using concrete-filled steel tubes. Because these joints were significantly stiffer than the main steel tubes, instability naturally tended to occur in the main steel tube. In cases where the main steel tube was filled with concrete, the influence of concrete strength might become more obvious. It is crucial for the joint to remain undamaged to achieve the ultimate bending resistance of the concrete-filled steel tubes, which far exceed the bending resistance of unfilled steel tubes.

The results also show that concrete with grade C25 is enough to provide the compressive resistance needed for the local strut-and-tie model in the CFST joint area. Because of this, using higher-strength concrete does not significantly increase the overall bending resistance of the mechanical joint. This highlights that the tensile strength mainly comes from the steel tube itself, not from stronger concrete. So, once the concrete strength reaches a minimum level to support local compression, using higher-grade concrete does not help much. Instead, the main factors that affect the bending performance of the CFST system are the steel tube's quality and geometry. This shows that for CFST joints, the steel part plays the key role in providing bending resistance, and concrete only needs to meet a basic strength level.

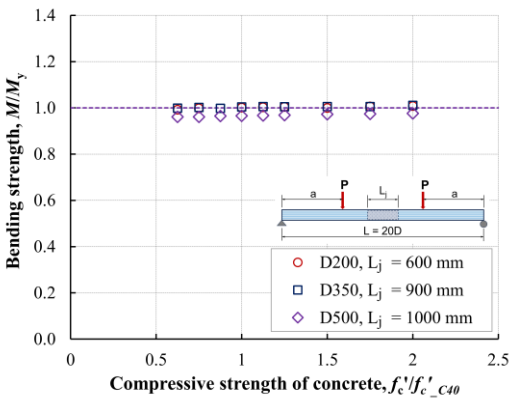

Fig. 15 Effects of compressive strength of concrete on bending strength

Similar to the compressive strength of concrete, analysis results also showed that the influence of the reinforcement ratio on the bending resistance of the structure could be negligible. Both longitudinal and spiral reinforcements were considered in this study. Fig. 16 presents the analysis results from models D200, D350, and D500, indicating that bending resistance remains nearly unchanged with varying reinforcement ratio in the concrete core. This finding aligned with a previous study on the effect of reinforcement on structural bending resistance [28]. It can be inferred that for concrete-filled steel tubes using mechanical joints, additional reinforcement may not be necessary as the steel tube and concrete core could provide sufficient resistance for the steel tube to achieve the ultimate bending capacity. However, in cases where the main steel tube is also filled with concrete, increasing the reinforcement content in the joint could significantly enhance the local resistance of the concrete core, reducing local cracking in the concrete within the tension zone and thereby stabilizing the joint.

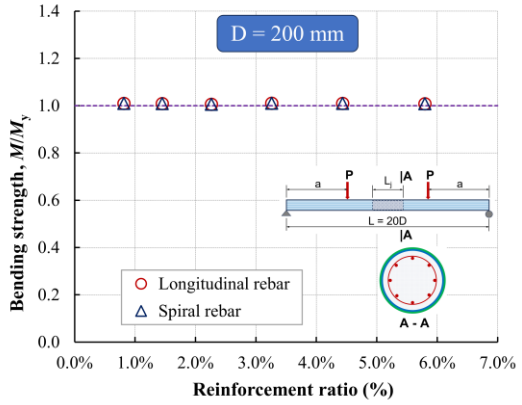

(a) D = 200 mm, L_j = 600 mm

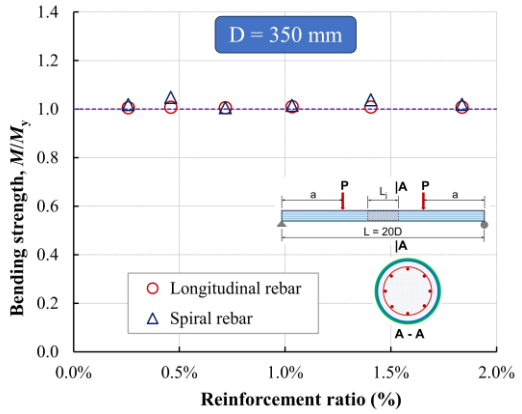

(b) D = 350 mm, L_j = 900 mm

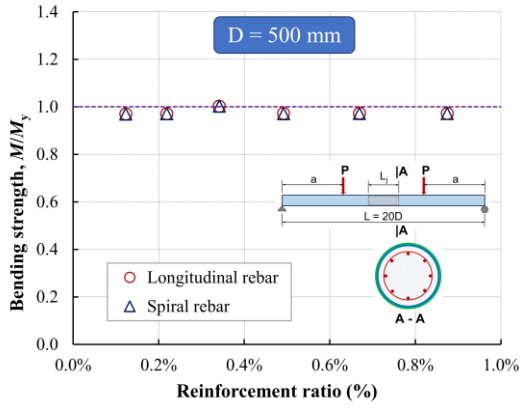

(c) D = 500 mm, L_j = 1,000 mm

Fig. 16 Effects of reinforcement ratio on bending strength

Shear connectors can be employed to prevent slips between main tubes and the connecting tube, as introduced in Fig. 1. Several types of connectors can be considered such as shear studs, steel ribs, and weld joints which will be further investigated in separate experimental studies of the mechanical joint. A finite element analysis was conducted for modal D200 to investigate the bending capacity of the steel tubes with the proposed mechanical joint. Elastic spring elements with appropriate stiffness were applied near the edges of the joint to simulate shear connectors that could partially fix relative displacement between tubes, and the concrete core. Fig. 17 presents comparative results in bending strength between a jointless tube and tubes with mechanical joint with and without shear connectors. The study revealed that the connectors slightly enhanced the structure's bending stiffness by reducing slips between components. At the rotation angle $\phi = \phi_y$, the bending strength with shear connectors was identical to that of a jointless tube and 8.6% greater than that of a structure without shear connectors. However, the impact on maximum bending strength was minimal, as the joint itself provided enough rigidity for the main tubes to reach their maximum capacity before failing due to local buckling.

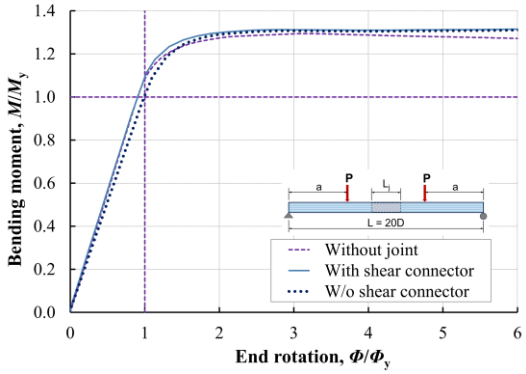

Fig. 17 Effect of anchoring interaction from using shear connectors

5. Design proportions and recommendations

The previous section introduced a strut-tie model with tension and compression areas to assess the local load-bearing capacity of concrete-filled steel tube joints. This tension zone was generated by frictional effects between the main tube and the connecting tube. Local shear force appeared at the contact surface due to friction, creating a longitudinal tensile stress field along the connecting tube. Fig. 18 presents the principal stress distribution at first yield within the joint steel tube and concrete core obtained from finite element analysis of models D200, D350, and D500. The tensile stress field concentrates along the bottom fiber of the steel tube, while the compressive stress field primarily dissipates within the concrete core. Based on such stress distribution, regions for tension and compression are identified and used to compute the structural load-bearing capacity.

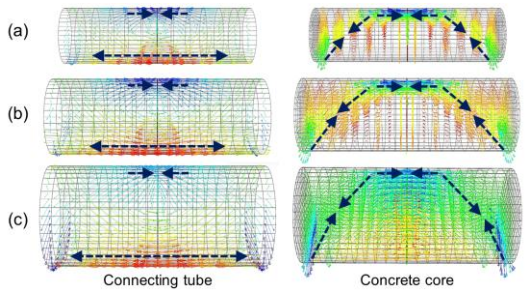

Fig. 18 Principal stress tensors in connecting tubes and concrete cores:

(a) D = 200 mm; (b) D = 350 mm; (c) D = 500 mm

Examining the stress tensor configurations revealed two distinct stress fields within the joint steel tube: tensile stresses along the bottom fiber and compressive stress in the top fiber of the cross sections. The tensile stress field was distributed along the connecting tube, while the compressive stress field was mainly located near the middle region of the joint. Observation of the stress field within the concrete core showed a distribution that aligned well with the proposed strut-tie model in this study. Two main compressive stress fields were generated within the concrete core: a diagonal compressive stress tensor from the bottom left and right edges toward the top fiber and a compressive stress tensor concentrated near the central region of the joint. It is obvious that the connecting steel tube and concrete core simultaneously generated compressive

resistance within the upper section of the joint. In addition, the infilled concrete was constrained by the steel tube, creating a triaxial compression state that could enhance both the strength and strain capacity of the concrete infill. Analysis results successfully verified the proposed theory in this study which can be utilized to compute the load-bearing capacity of mechanical joints using concrete-filled steel tubes based on the strut-tie model. The strut-tie phenomenon became more obvious when the length-to-diameter ratios L_j / D of the joint were less than 3.0. Findings from this study were consistent with those from Lu et al. [11] who proposed a strut-tie model and corresponding effective areas to describe the load transfer mechanism in the circular composite member under pure bending conditions.

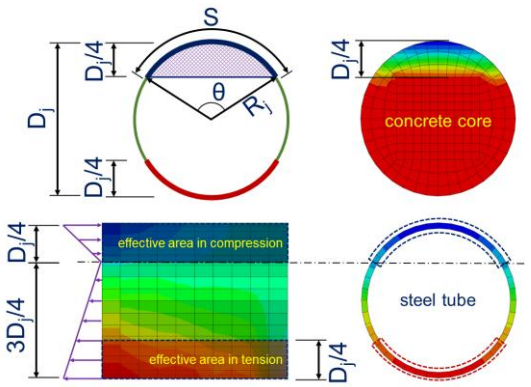

Fig. 19 Effective area of concrete core in compression at first yield

This study focused on developing a method to assess local strengths of the mechanical joint by introducing an approximate theory based on the analysis results to calculate strut and tie strength. Effective cross sections were proposed to define the compression and tension resistances based on the strut-tie model. From finite element analyses, it was found that the compression stress was almost similarly distributed in the range of D_j /4 from the top fiber for all models D200, D350, and D500. Fig. 19 shows the typical stress distribution in the cross section in which the effective areas can be simply defined. The cross section of the joint contributing to compression resistance is considered as a circular segment within D_j /4 from the extreme top fiber. The effective area in compression of the steel tube segment contributing to compression resistance can be proposed as

$$A_{s,c} = \theta D_j t_j / 2 \tag{6}$$

where, $\theta = 2\arcsin\left(\sqrt{3}/2\right)$.

The effective area in compression of the concrete core is equal to the area of the circular segment minus the arc-length area of the steel tube:

$$A_c = \frac{D_j^2}{8}\left(\theta - \sin\theta\right) - A_s \tag{7}$$

The total axial compressive strength of the whole circular segment is defined as follows:

$$S_{2,n} = F_y A_{s,c} + 0.85 f_c^{'} A_c \tag{8}$$

Similarly, the active section in tension of the connecting steel tube to resist the tie force can be assumed as the arc segment in the range of D_j /4 from the bottom extreme fiber as illustrated in Fig. 21. The effective area is defined from the arc-length area as follows:

$$A_{s,t} = \theta D_j t_j / 2 \tag{9}$$

The axial tensile strength of the steel arc segment is defined as follows:

$$T_n = F_y A_{s,t} \tag{10}$$

From the proposed theory of the strut-tie model as presented in Fig. 4, diagonal strut forces were defined from the acting of couple generated by the internal bending moment in main tubes. Several research have successfully developed and proposed theories to define the effective section of the diagonal strut for deep beam [24- 26]. However, most theories only focus on strut-tie models for reinforced concrete beams with rectangular sections. This study observed stress distribution in circular concrete cores from a series of analysis models to find the effective section for the diagonal strut. It was found that compressive stress flow was transmitted through an effective section of an equivalent cylinder as illustrated in Fig. 20. As the length-to-diameter ratio of the joint decreased, the deep-beam effect and the diagonal stress flow became more obvious. In this study, a method to determine the effective concrete section in the strut-and-tie model was proposed. Specifically, the authors selected an equivalent circular section with a diameter $d_e = D_j$ /3 where D_j is the diameter of the CFST joint. This simplification allows for easier calculation of the compression resistance of the diagonal strut within the strut-tie model. The axial compression resistance of the diagonal strut can be obtained as:

$$S_{1,n} = 0.85 f_c^{'} (\pi d_e^2) / 4 \tag{11}$$

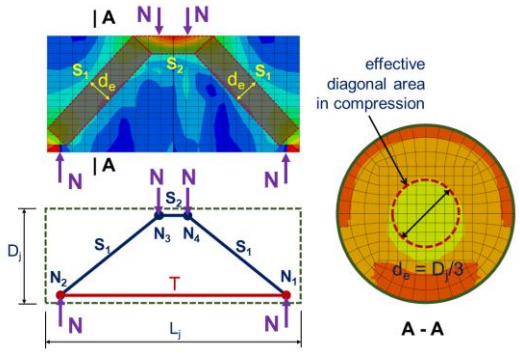

Fig. 20 Assumed effective diagonal area in compression

Local failures of the concrete core at node locations (N_1 to N_4) must be secured by controlling local stresses due to radial pressure Δp generated by couple N as presented in Fig. 20. The magnitude of the radial pressure must not exceed the compressive strength of the concrete. As presented in Fig. 4, the magnitude of Δp can be determined based on the mechanism of the shrink-fit joint [34].

From the previous section, the proportion for connecting length of the mechanical joint was successfully confirmed. To ensure the transmission capacity for the bending moment of the joint, the active length L_j of the joint should be at least three times the diameter D of the main tubes. Findings from this study were consistent with previous achievements in slip joints of towers for offshore wind turbines and power transmission.

Another proportion of the effective thickness of the connecting tube was also proposed. The thickness of the connecting steel tubes should not be less than the thickness of the main tubes, $t_j \geq t$, to secure the rigidity so that the bending moment from main tubes could be completely transmitted through the joint. The connecting steel tube not only provided confining effect for the infilled concrete but also contributed to the tension resistance and compression resistance of the joint based on the strut-tie model theory.

This study also investigated the effects of the compressive strength of the concrete core and the contribution of steel reinforcement on the performance of the mechanical joint. Although variation in concrete strength and reinforcement ratio did not obviously affect the capability of the main tubes for reaching the critical strength since the joint itself could provide sufficient rigidity regardless of the concrete strength, the main tubes completely failed due to local buckling of circular ring in compression. Therefore, the compressive strength of the concrete core is defined by securing the axial compression strength of the strut members under local strut forces. Similarly, the use of steel reinforcement can be neglected in the bending design of the mechanical joint using CFST.

6. Conclusions

The investigation into mechanical joints using CFST offers a promising advancement in structural engineering, particularly for applications involving steel tube structures. This study introduced a new mechanical joint using CFST to enhance construction efficiency by eliminating the need for site welding, thereby maintaining continuity and ensure instant load-bearing capacity post-installation. Key parameters such as the length and thickness of the connecting tube, compressive strength of the concrete core, and reinforcement steel ratio

were extensively analyzed to establish design recommendations. Shear connectors could improve the interaction between the steel tubes and concrete core and structural integrity during load bearing to prevent slip and global deformation. These findings are critical for simplifying construction practices and optimizing joint performance that might enable more effective and efficient use of CFST in various structural applications. Beyond its technical performance, this innovative mechanical joint design also brings substantial economic and logistical advantages. By eliminating the need for on-site welding, construction time is significantly reduced, resulting in faster project delivery and lower labor costs. Furthermore, the design is well-suited to prefabrication, which minimizes site work and improves quality control. Together, these factors lead to significant cost savings and enhanced construction efficiency, making CFST joints an attractive choice for rapid, reliable, and cost-effective structural applications.

To enhance the reliability and applicability of the findings presented in this study, further research is recommended to validate and refine the theoretical models. Future experimental investigations should be conducted to assess the actual performance of the proposed mechanical joint under realistic loading conditions. These studies should focus on verifying theoretical predictions related to bending strength, stiffness, and overall structural behavior of CFST joints.

Moreover, additional research should aim to develop comprehensive design guidelines and contribute to the formulation of new standards for the implementation of the proposed mechanical joint in structural applications. Investigations into the influence of material properties, joint configurations, and varying loading conditions are also necessary to fully understand the behavior and limitations of the proposed joint design. Furthermore, numerical simulations with advanced modeling techniques should be explored to enhance predictive accuracy and optimize design parameters for practical applications.

Acknowledgements

The authors would like to express their gratitude to Ho Chi Minh City University of Technology (HCMUT) – Vietnam National University Ho Chi Minh City (VNU-HCM) for their valuable support in this study.

References

[1] Ishii T., Fujisawa S., and Ohmori A., "Overview and application of steel materials for high-rise buildings", JFE Technical Report, 14(14), 1-8, 2000.
[2] Gao S., Usami T., and Ge H., "Ductility evaluation of steel bridge piers with pipe sections", Journal of Engineering Mechanics, 124(3), 260-267, 1998.
[3] Yasunami H., Terada M., Natori T., and Murakoshi, J, "Numerical Simulation of Steel Pipe Column with Outer Pipe for Seismic Retrofit", Steel Construction Engineering, 5(19), 85-96, 1998.
[4] Shinohara M., Kanaji H., Oniki K., and Kimura, M., "A Proposal of a Bridge Column integrated by Multiple Steel Pipes with Directly-Connected Piles and a Seismic Response Analysis", Journal of Japan Society of Civil Engineers, Ser: C (Geosphere Engineering), 69, 312-325, 2013.
[5] Huo S., Chao Y., Dai G., and Gong, W., "Field test research of inclined large-scale steel pipe pile foundation for offshore wind farms", Journal of Coastal Research, 73, 132-138, 2015.
[6] Li X., Dai G., Zhu M., and Gong, W., "Application of static loading tests to steel pipe piles with large diameters in Chinese offshore wind farms", Ocean Engineering, 186, 106041, 2019.
[7] Segeren M.L., Lourens E.M., Tsouvalas A., and Van Der Zee T.J., "Investigation of a slip joint connection between the monopile and the tower of an offshore wind turbine", IET Renewable Power Generation, 8(4), 422-432, 2014.
[8] Cabboi A., Kamphuis T., Van Veldhuizen E., Segeren M., and Hendrikse H., "Vibration-assisted decommissioning of a slip joint: Application to an offshore wind turbine", Marine Structures, 76, 102931, 2021.
[9] Li G.C., Chen B.W., Yang Z.J., Liu Y.P., and Feng, Y.H., "Experimental and numerical behavior of eccentrically loaded square concrete-filled steel tubular long columns made of high-strength steel and concrete", Thin-Walled Structures, 159, 107289, 2021.
[10] Nakamura S.I., Momiyama Y., Hosaka T., and Homma K., "New technologies of steel/concrete composite bridges", Journal of Constructional Steel Research, 58(1), 99-130, 2002.
[11] Lu H., Han L.H., and Zhao X.L., "Analytical behavior of circular concrete-filled thin-walled steel tubes subjected to bending", Thin-Walled Structures, 47(3), 346-358, 2009.
[12] Moon J., Roeder C.W., Lehman D.E., and Lee, H.E., "Analytical modeling of bending of circular concrete-filled steel tubes", Engineering structures, 42, 349-361, 2012.
[13] Cho J., Moon J., Ko H.J., and Lee, H.E., "Flexural strength evaluation of concrete-filled steel tube (CFST) composite girder", Journal of Constructional Steel Research, 151, 12-24, 2018.
[14] Lehman D.E., and Roeder C.W., Rapid construction of bridge piers with improved seismic performance, Department of Civil Engineer, University of Washington, 2012.
[15] Moon J., Lehman D.E., Roeder C.W., and Lee H.E., "Strength of circular concrete-filled tubes with and without internal reinforcement under combined loading", Journal of Structural Engineering, 139(12), 04013012, 2013.
[16] Stephens M.T., Lehman D.E., and Roeder C.W., "Design of CFST column-to-foundation/cap beam connections for moderate and high seismic regions", Engineering Structures, 122, 323-337, 2016.
[17] Chin W.J., Kang J.Y., Choi E.S., and Lee J.W., "Study on structural behavior characteristics of concrete filled steel tube girder bridges", Korea Institute of Construction Technology, Goyang, Republic of Korea, 2008.
[18] Ichikawa K., Sato R., and Terao N., "Development of Mechanical Joint New "High-Mecha-Neji" for Steel Pipe Piles and Steel Pipe Sheet Piles", JFE Technical Report, No. 25: 9-16, 2020.
[19] Akutagawa H., Takano K., and Tajika H., "Mechanical Joint "KASHEEN" for Large-Diameter Pipe Piles", JFE Technical Report, No. 8: 51-56, 2006.
[20] Masashi K., Yoshiro I., Hironobu M., Yoshinori F., Toshihiko S., Shinji T., Tadachika M., and Hiroyuki T., "Development of the Mechanical "Gachi-cam Joint" for Steel Pipe Piles and Steel Pipe Sheet Piles", Nippon Steel & Sumitomo Metal, Technical Report, No. 113: 34-41, 2016.
[21] Fu Z., Ji B., Maeno H., Eizien A., and Chen J., "Flexural behavior of lightweight aggregate concrete filled steel tube", Advanced Steel Construction, 10(4), 385-403, 2014.
[22] Li G., Qiu Z., Yang Z., Chen B., and Feng Y., "Seismic performance of high strength concrete filled high strength square steel tubes under cyclic pure bending", Advanced Steel Construction, 16(2), 112-123, 2020.
[23] Yang Z-J., Zhang S., Cui W-Z., and Li G-C., "Flexural behavior of reinforced hollow high strength concrete filled square steel tube", Advanced Steel Construction, 20(2), 199-207, 2024.
[24] Park, J.W., and Kuchma, D., "Strut-and-tie model analysis for strength prediction of deep beams", ACI Structural Journal, 104(6), 657, 2007.
[25] El-Zoughiby M.E., El-Metwally S.E., Al-Shora A.T., and Agieb E.E., "Strength prediction of simply supported R/C deep beams using the strut-and-tie method", Arabian Journal for Science and Engineering, 38, 1973-1991, 2013.
[26] Shuraim A.B., "Behavior and shear design provisions of reinforced concrete D-region beams", Journal of King Saud University-Engineering Sciences, 25(1), 65-74, 2013.
[27] Tuchscherer R.G., Birrcher D.B., Williams C.S., Deschenes D.J., and Bayrak O., "Evaluation of Existing Strut-and-Tie Methods and Recommended Improvements", ACI Structural Journal, 111(6), 2014.
[28] Tuan N.C., and Khiem N.T., "A numerical analysis on bending capacity of steel pipe columns using a mechanical joint with concrete-filled steel tube", Journal of Science and Technology in Civil Engineering (JSTCE)-HUCE, 16(4), 87-99, 2022.
[29] Roeder C.W., Lehman D.E., and Bishop E., "Strength and stiffness of circular concrete filled tubes", Journal of Structural Engineering, 136(12), 1545–1553, 2010.
[30] AASHTO LRFD Bridge Design Specification, The American Association of State Highway and Transportation Officials, Washington DC, USA, 2010.
[31] AISC Specification for structural steel buildings, AISC, Chicago, IL; 2010.
[32] ACI Building code requirements for structural concrete and commentary, ACI318-08, Farmington Hills, MI, 2008.
[33] Design of composite steel and concrete structures - Part 1.1: general rules and rules for buildings, Eurocode 4, European Committee for Standardization, Brussels; 2004.
[34] Firouz-Abadi R.D., Mehralian F., Amirabadizadeh H., and Yousefi M., "A Novel Approach to Model the Shrink-Fit Connection", In International Conference on Rotor Dynamics (pp. 25-35), Springer International Publishing, 2023.
[35] Slocum R., and Fairbairn M., "Slip Joints Connections - How Do These Things Work?", In Electrical Transmission and Substation Structures, 363-374, 2015.
[36] Mojto M., Brodnianský J., Recký J., and Tilinger, M., "Modelling and experimental tests of spatial structure focused on slip joints", In Proceedings of International Association for Shell and Spatial Structures (IASS), 18, 1-9, 2020.
[37] ABAQUS standard user's manual version 6.5, Hibbit, Karsson and Sorensen Inc., 2005.
[38] Nolle H., and Richardson R.S.H., "Static friction coefficients for mechanical and structural joints", Wear, 28(1), 1-13, 1974.
[39] Baltay P., and Gjelsvik A., "Coefficient of friction for steel on concrete at high normal stress", Journal of Materials in Civil Engineering, 2(1), 46-49, 1990.
[40] Rabinowicz E., and Tanner R.I., "Friction and wear of materials", Journal of Applied Mechanics, 33(2), 479, 1966.
[41] Fuller D.D., Coefficients of friction, American Institute of physics handbook, 1972.
[42] Blau P.J., Friction science and technology: from concepts to applications, CRC press, 2008.
[43] Hutchings I., and Shipway P., Tribology: friction and wear of engineering materials, Butterworth-heinemann, 2017.
[44] Lubliner J., Oliver J., Oller S., and Oñate E., "A plastic-damage model for concrete", International Journal of solids and structures, 25(3), 299-326, 1989.
[45] Grassl P., and Jirásek M., "Damage-plastic model for concrete failure", International journal of solids and structures, 43(22-23), 7166-7196, 2006.
[46] Sarikaya A., and Erkmen R.E., "A plastic-damage model for concrete under compression", International Journal of Mechanical Sciences, 150, 584-593, 2019.
[47] Wong M.B., Plastic analysis and design of steel structures, Burlington (MA), Butterworth, 2009.
[48] Lubliner J., Oliver J., Oller S., and Oñate E., "A plastic-damage model for concrete", International Journal of Solids and Structures, 25, 299–329, 1989.
[49] Lee J., and Fenves G.L., "Plastic-damage model for cyclic loading of concrete structures". Journal of Engineering Mechanics, ASCE, 124(8), 892–900, 1998.
[50] Kiessling F., Nefzger P., Nolasco J.F., and Kaintzyk U., Requirements on loading and strength. In: Overhead Power Lines, Power Systems, Springer, Berlin, Heidelberg, 2003
[51] Slocum R., and Fairbairn M., "Slip Joints Connections - How Do These Things Work?", Electrical Transmission and Substation Structures, 363-374, 2015.
[52] Brodniansky J., Recký J., Magura M., Klas T., and Botló M., "Slip joint connection of conical towers subjected to bending and torsion", Advances and Trends in Engineering Sciences and Technologies III, 55-60, CRC Press, 2019.
[53] Mojto M., and Cabboi A., "The mechanical behaviour of a slip joint for an offshore wind turbine: First monitoring and modelling results", Thin-Walled Structures, 196, 111482, 2024.